Tuning the Energy Landscape of Soft Robots for Fast and Strong Motion

Jiefeng Sun[1], Brandon Tighe[1], and Jianguo Zhao[1]

Abstract— Soft robots demonstrate great potential compared with traditional rigid robots owing to their inherently soft body structures. Although researchers have made tremendous progress in recent years, existing soft robots are in general plagued by a main issue: slow speeds and small forces. In this work, we aim to address this issue by actively designing the energy landscape of the soft body: the total strain energy with respect to the robot's deformation. With such a strategy, a soft robot's dynamics can be tuned to have fast and strong motion. We introduce the general design principle using a soft module with two stable states that can rapidly switch from one state to the other under external forces. We characterize the required triggering (switching) force with respect to design parameters (e.g., the initial shape of the module). We then apply the soft bistable module to develop fast and strong soft robots, whose triggering forces are generated by a soft actuator – twisted-and-coiled actuator (TCA). We demonstrate a soft gripper that can hold weights more than 8 times its own weight, and a soft jumping robot that can jump more than 5 times its body height. We envision our strategies will overcome the weakness of soft robots to unleash their potential for diverse applications.

I. INTRODUCTION

Soft robots can interact with environments and humans in simplified, safer, and adaptive ways owing to their body compliance [1]. However, they usually cannot generate large forces also due to body compliance, thus unable to realize fast motion. Although some soft robots can realize rapid motions [2]–[6], they require an intensive power input. But intensive power inputs may not be always possible due to limited capability of actuators such as motors, compressors, and especially artificial muscles, or sometimes due to limited power supply, especially when a robot is untethered. To address this problem, in this work, we leverage the internal energy stored in a soft robot to realize strong and fast motion without an intensive power input and strong actuators.

Our proposed strategy is to actively design the energy landscape for a soft robot, which is the total strain energy in the robot with respect to its deformation (e.g., bending angle for a soft manipulator). The energy landscape for a traditional soft robot in general is monostable, i.e., it only has one minimum, corresponding to a single stable state (Fig. 1a). When deformed under external actuation, the robot will return to this state if the actuation is removed. We propose to tune the energy landscape to achieve two local minima (details in section II), corresponding to two stable
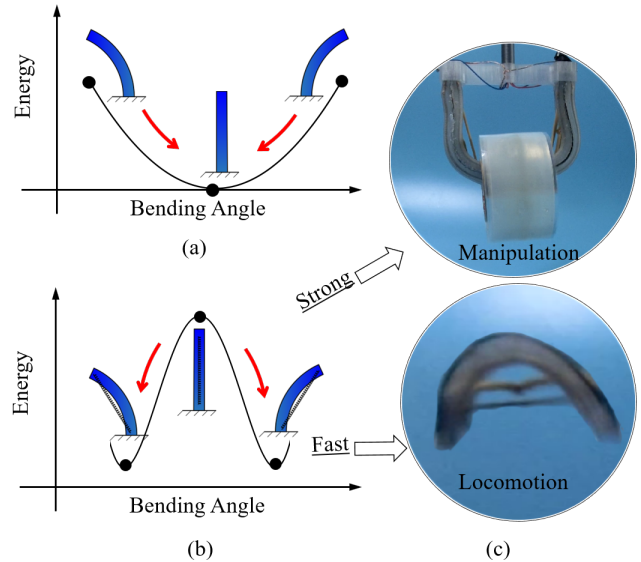
Fig. 1: The proposed strategy for shaping the energy landscape of soft robots to enable fast and strong motion. (a) The energy landscape for traditional soft robots has one energy minimum corresponding to one stable state. (b) The energy landscape can be tuned to have two minima corresponding to two stable states. (c) Such a strategy can be used for strong manipulations and fast locomotion.

states (Fig. 1b) by adding an additional elastic element (e.g., springs). To switch from one stable state to the other, the soft body needs to first store energy to surpass an energy peak, after which the stored energy can be released to generate fast motion. With such bistable designs, the dynamics for a soft robot can be actively tuned for strong manipulation and fast locomotion (Fig. 1c and the supporting video).

Our proposed strategy belongs to a more general framework called bistable or multistable mechanisms, for which a mechanism has two or more stable states. Such a strategy has recently been exploited in various areas beyond soft robots. For instance, it has been used to develop bio-inspired spring origami for shape morphing [7], dual stiffness structures for aerial robots [8], deployable structures [9], metamaterials for shock absorption [10], bistable valves to control air flow [11], and legs for swimming robots [12]. However, most of the existing mechanisms rely on both rigid and soft components to design compliant bistable mechanisms [13]. It remains largely unknown on how to exploit the bistablity for soft robots to enable fast and strong motion.

In this paper, we aim to investigate how to tune the energy landscape for desired stable states (bistable or monostable) for a soft module. This is accomplished by two competing potential energies in two energy-storing components: 1) potential energy in a linear spring attached to the body; 2) potential energy generated by the bending of the soft body. By actively designing these two energies, the total energy landscape for the module can be tuned to achieve a desired shape: symmetrically bistable (SB), asymmetrically bistable (AB), and monostable (MS). Using a soft actuator – twisted-and-coiled actuator (TCA) to actuate the module, we demonstrate the application of the AB type energy landscape: a soft gripper that can hold weights more than 8 times of its own weight, and a soft jumping robot that can jump more than 5 times its body height.

There are two main contributions of the paper. First, we propose a strategy to enhance the performance of soft robots: actively designing the energy landscape. We also perform detailed analysis using the finite element analysis (FEA) for how to implement the strategy. Second, we implement the proposed strategy and demonstrate its effectiveness by developing soft robots for manipulation (grasping) and locomotion (jumping) as shown in Fig. 1c. Such robots are driven by a light-weight and electrical-driven TCAs [14], [15], which can potentially be used for untethered locomotion [16].

The rest of this paper is organized as follows. We first introduce the working principle of the strategy to tune an energy landscape in section II. Then, we elaborate the materials selection and fabrication procedures for a soft bending module in section III. After that, we describe the FEA modeling and characterization of the module in section IV. Finally, in section V, we apply the soft module to develop a gripper and a jumping robot to demonstrate the effectiveness of the proposed strategy.

II. WORKING PRINCIPLE

In this section, we introduce the working principle using a soft bending module. As shown in Fig. 2, the module has a flexible plastic sheet sandwiched between two soft bodies. Each soft body has two parallel channels to host an actuator, which can be a cable or a TCA. A linear spring is attached on the plastic sheet, and can freely move through a large hole in the plastic sheet when the module bends. The plastic sheet can have various initial shapes, i.e., it can either have an initially straight or curved shape. The spring can have various lengths and stiffness before attaching to the plastic sheet.

With such a design, we can tune the energy landscape for the module since the total energy is mainly comprised of two major components: potential energy from bending the soft body (bending potential energy), potential energy from stretching the spring (stretching potential energy). Such two components can be individually tuned by designing the initial shape of the plastic sheet and the initial length and stiffness of the spring. To illustrate the principle, we use a simplified linear model in this section, and a more accurate
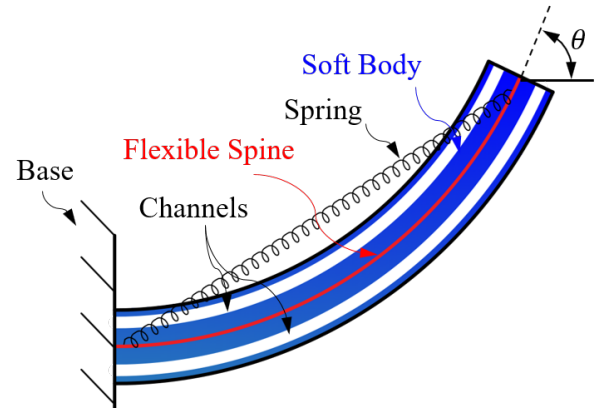

Fig. 2: Schematic of the proposed soft bending module with tunable energy landscapes.

model using finite element analysis (FEA) will be introduced in section IV.

Both the bending and stretching energies can be approximated using functions with respect to the bending angle θ as in Fig. 2. Assume the initial shape of the plastic sheet is at a bending angle θ_0, the strain energy stored in the sheet due to bending with respect to θ is

$$U_b = \frac{1}{2}k_b(\theta - \theta_0)^2 \qquad (1)$$

where k_b is the effective bending stiffness of the sheet and the body. The stretching strain energy in the spring is

$$U_l = \frac{1}{2}k_l(\Delta L)^2, \qquad (2)$$

where k_l is the linear stiffness of the spring, ΔL is the length change of the spring, which can be written as a function of θ

$$\Delta L = \frac{2L_{max}}{\theta}sin(\frac{\theta}{2}) - L_{in}$$

where L_{max} is the maximum length of the spring when the module bends, and L_{in} is the initial length of the spring under no load. The total energy for the module is thus

$$U_{tot} = U_b + U_l = \frac{1}{2}k_b(\theta - \theta_0)^2 + \frac{1}{2}k_l(\Delta L)^2, \qquad (3)$$

With the two potential energies, we can design the energy landscape of the module U_{tot} to achieve three different interesting cases: symmetric bistable (SB), asymmetric bistable (AB), and monostable (MS).

- SB (Fig. 3a): The soft body is initially designed to be straight (i.e., $\theta_0 = 0$). In this case, the bending potential energy is a parabola with the minimum value at zero bending angle. Combining this energy profile with the stretching potential energy, we obtain a symmetric profile for the total energy.
- AB (Fig. 3b): The soft body is initially designed to be bent at an angle (i.e., $\theta_0 \neq 0$). Therefore, the bending potential energy will be shifted to the right, while the stretching potential energy will be the same. Combining these two energies together, we obtain an asymmetric
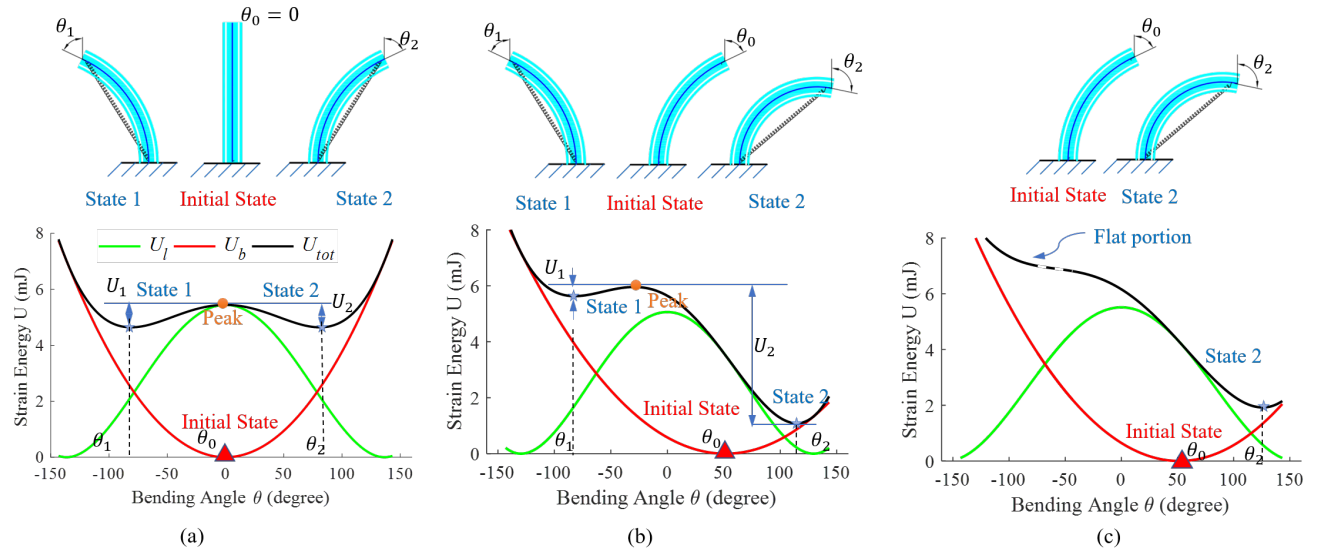
10083

Fig. 3: Different configurations of the energy landscape for a soft bending module. (a) Symmetric bistable (SB). (b) Asymmetric bistable (AB). (c) Monostable (MS).

energy profile with the left energy barrier (the energy difference in height between a local minimum and a neighboring energy peak) much smaller than the right one. In this case, it will be easier to switch from state 1 to state 2 owing to a smaller energy barrier.

- MS (Fig. 3c): By properly adjusting the peak value for the stretching potential energy, the left stable state (state 1) can disappear, leaving only state 2 as the single minimum for the total potential energy. In this case, the system is monostable.

Each of the three types of energy landscapes has its own advantages compared with a normal bending module without a spring. An SB module (Fig. 3a) has a flat portion around the energy peak and two stable states. In this way, an SB module can store/release energy in the bending process, generating faster dynamics after the energy peak. An SB module may be used for robots that require faster symmetrical oscillatory motion (e.g., the repetitive bending motion in a robotic fish).

An AB module has an obvious advantage: a small energy input will allow it to pass the energy peak from state 1 to state 2, releasing a larger amount of stored energy than the input energy. This advantage can be interpreted in two perspectives. In terms of dynamics, the larger released energy will shape the dynamics of the soft body to generate a relatively fast motion after the energy peak. In this case, it can be used for robot locomotion requiring an instant release of a large amount of energy (e.g., jumping [17]). On the other hand, in terms of statics, the module initially in state 2 will need a larger force to switch to state 1 compared with an SB module. In this case, an AB module is ideal for robotic fingers that can passively hold some weights.

An MS module's energy landscape could have a flat portion that means the stiffness of the module becomes almost zero, and it does not require energy for the module to bend more. In this case, the module will bend fast when

the driven force from the actuators is constant.

Although the proposed soft module contains a plastic sheet, it still preserves the most important features of soft robots – a continuum body that has infinite degrees of freedom, safe to humans, and resilient to harsh conditions. We can find similar examples in the biological world. Serpentes (snake) families with extraordinary dexterity have inspired many soft robots with this kind of structure – flexible spinal columns made up of many vertebrae and ligaments that can store energy. So, in the following, we refer the plastic sheet as a flexible spine.

III. MATERIALS AND FABRICATION

A bending module is composed of the components as shown in Fig. 4(a), including: two TCAs (it can also be cables), two soft bodies with channels, a flexible spine, and a spring. Since the fabrication processes for different types of modules are similar, we illustrate the detailed fabrication process with the SB module.

The actuator TCA is an artificial muscle that will contract or extend [18] when subjected to Joule heating using electricity. It is low-cost compared to the more prevalent artificial muscles such as the shape memory alloy (SMA) and shape memory polymer. The TCA can contract by over 50% after heating, lift loads over 100 times heavier than can human muscle of the same length and weight [19]. The detailed treatment of TCAs can be found in [19]. We use a recently improved method to fabricate TCAs with the following geometry parameters: Outer diameter 1 mm, inner diameter 0.4 mm [20].

The fabrication of the bending module comprises three major steps. 1) Fabricate the flexible spine. The flexible spine is directly printed in a flat shape using a 3D printer (Prusa M3K3) with NylonX (MatterHackers Inc.). 2) Fabricate the soft body. The soft body is fabricated through the standard
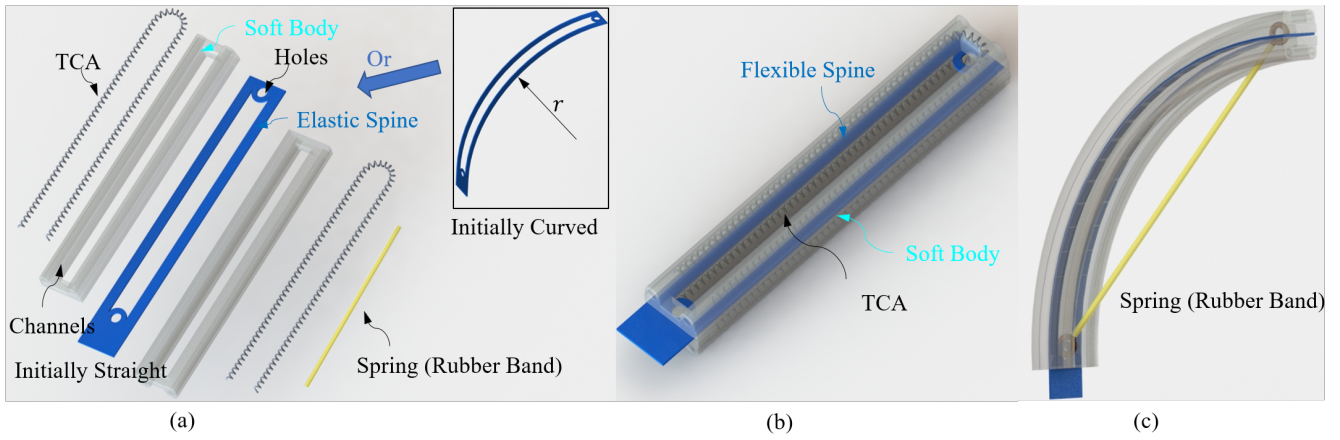
Fig. 4: Fabrication process of the module. (a) All the components except the spring are assembled together to generate a complete module in (b). The spring is finally attached to the spine in (c).

molding method [21] for soft robots by curing mixed liquid EcoFlex-30 (Smooth-On, Inc.) in a 3D printed mold. We create channels by inserting carbon fiber rods into the mold, which are removed before demolding. 3) Assemble all the components. The spine and the soft bodies are combined together using Sil-Poxy Silicone Adhesive (Smooth-On Inc.) in Fig. 4b. After that, a folded rubber band with a length of 32 mm (Standard size 19, width = 1/16") is attached to the holes in the flexible spine as in Fig. 4c. Finally, We insert TCAs into the two channels in the soft body to form a U-shape to generate a large actuation force. Extra silicone adhesive is applied to fix the two electric leads of the TCA on the soft body. The dimension for a straight module (Fig. 4b) is $45 \times 10 \times 8$ mm, and the thickness of the spine is 0.35 mm. We select NylonX, a nylon filament reinforced by adding micro-carbon fibers, to print the spine for two reasons. First, it retains the durability and flexibility of Nylon. Second, it can also retain its shape and stiffness when TCAs are thermally actuated as NylonX has a high heat deflection temperature (150°C).

An AS soft module is fabricated by using an initially curved flexible spine in step (2), which is shown in the inset of Fig. 4a. We fabricate an initially curved spine from the flat one. First, we tape a flat spine to a heat-resistant cylinder (beakers) to form an arc shape. Then, we heat the spine over its glass transition temperature (180°C). The spine will keep the arc shape after cooling down and removing the tapes. We can use beakers of various diameters to fabricate spines with different initial curvatures.

IV. SIMULATION AND CHARACTERIZATION

The simplified model for energy analysis in section II is used to illustrate the working principle. In this section, we utilize FEA to perform detailed simulations and compare it with experimental results for a single module.

A. Model Using Finite Element Analysis

For FEA simulations, we want to see how much force is required to trigger the switching of the module, and how

the initial bending angle θ_0 will influence the triggering force, which is the maximum force required for an actuator to switch the module's states. Since an AB module can be driven with any soft actuator such as cable, TCA, or SMA, here we assume the module is driven by cables to simplify the experimental procedure.

We conduct the FEA with Abaqus 6.14 (Dassault Systèmes Simulia Corp). The model can be simplified into 2D, and thus only a beam element type (B21) is used. The FEA model uses a spine of rectangular shape that has the same effective bending stiffness of the spine plus the soft body by specifying the young's modulus of the spine to be $E_{eq} = (E_b A_b + E_s A_s)/A_s$, where E_b and E_s are the young's modulus, and A_b and A_s are the cross-section areas of the body and the spine, respectively. To simplify the model, we use discrete channels instead of a continuous one. The main difference between the two is that the discrete channel will have limited points contacting the cable. Discrete channels are also simulated using a set of beam elements as shown in Fig. 5. The cable is also modeled with the beam element. A kinematic coupling interaction is used to attach the cable to the tip of the spine. A contact is established between the cable and the discrete channel. The spring is modeled with an Axial connector element (CONN3D2), with its two ends attached to the two nodes of the spine. We use a force stand (MARK-10, ESM303 stand & M5-2 force gauge) to obtain a force-displacement relationship of the spring and input it to Abaqus. As a boundary condition, the bottom of the spine is fixed.

In a simulation, there are two load steps. (1) A static step that allows the spring balances with the flexible spine to reach a steady state. (2) A dynamic step analysis applies a pulling displacement with a slow speed as a boundary on the cable that will trigger the switching of states. The triggering force is the maximum force from the force-displacement curve of the cable recorded during the simulation.
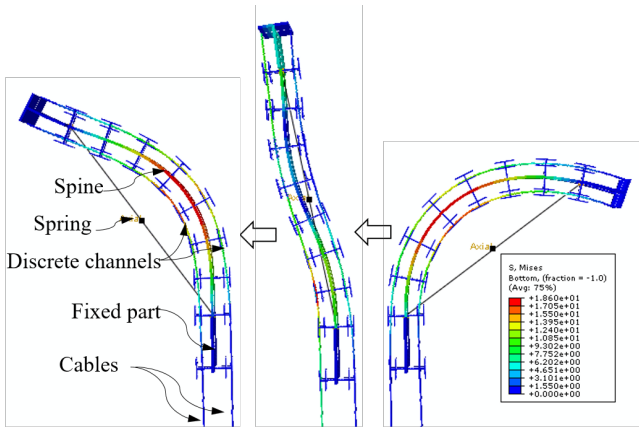
10085

Fig. 5: Different states in the FEA simulation.

B. Experiments and Comparison

We experimentally test the triggering forces for different bending modules with different initial curvatures and compare the experimental results with those generated from FEA. For the experiments, we use cables to apply the force (F_1 on the left and F_2 on the right, Fig. 6a). When switching from state 1 to state 2, we let $F_1 = 0$ and gradually increase F_2. In this case, the module starts to bend toward the right side (state 2). When F_2 is increased to a threshold value, F_{t2}, the module passes through the critical point and bends automatically to the right side (state 2). F_{t2} will be the triggering force from state 1 to state 2. Similarly, to switch from state 2 to state 1, we let $F_2 = 0$ while gradually increase F_1, and we record the triggering force F_{t1}.

Both F_{t1} and F_{t2} depend on the geometry of the module. We characterize the influence of the spine's initial angle θ on the switching force of an AB module and compare the experimental results with simulation results. The five different initial shapes are chosen to have an initial angle of $45°$, $50°$, $65°$, $75°$ and $100°$ (Fig. 6b), since we use different beakers available to us to fabricate the spines. All of them are fabricated from a flat shape with the same dimensions. In the experiments, a force testing stand (ESM303 stand with M5-2 force gauge, MARK-10) is used to drag the corresponding cable slowly (100 mm/min) until the states are switched and the maximum force during the process is recorded as the triggering force. A complete testing process can be found in the supporting video.

The simulation and experimental results are plotted in Fig. 6(c). As the initial bending angle θ_0 increases, F_{t1} increases and F_{t2} decreases, meaning it becomes more and more difficult to switch from state 2 to state 1, while it is easier to switch from state 1 to state 2. F_{t2} is almost zero when $\theta = 100°$, suggesting the module becomes monostable with only the stable state 2 since it does not require a force to switch to state 2. The experimental and simulation results match each other with a mean error of 0.15 N. The relatively large error for F_{t2} with $45°$ and $50°$ might be due to the friction force between the cable and the channel since we use a discrete channel instead of a continuous one.
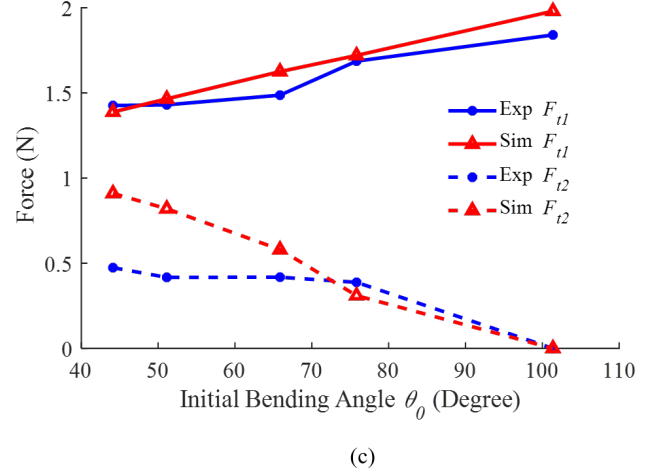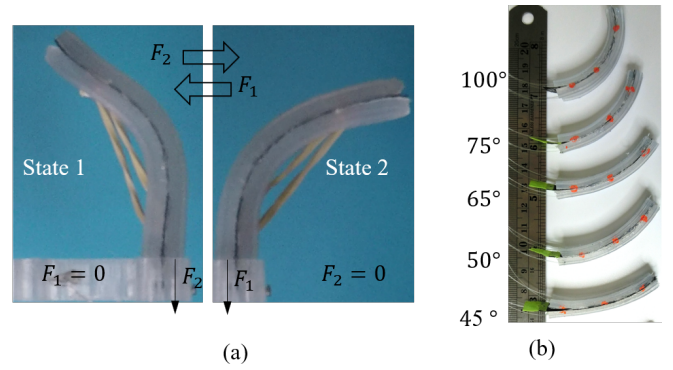

(a)

(b)

(c)

Fig. 6: Characterization of the soft bending modules. (a) The two stable states with labeled forces for switching the states. (b) Five modules with different initial bending angles. (c) Simulation and experimental results for the triggering forces to switch the state.

V. APPLICATION

To demonstrate the usefulness of the proposed strategy, we develop a soft robotic gripper with two modules as the fingers and a jumping robot with a single module. In this section, we describe the design and experiments for these two robots.

A. A Soft Gripper with Two Bistable Bending Modules

For the gripper, we design the two fingers as two AB modules (Fig. 7) to make it difficult to open while easy to close so that it can hold weights without additional energy input or hold heavier weights with some additional energy. We actuate the two fingers with TCAs as tendons, with each finger having two TCAs (TCA1 and TCA2 for left finger, and TCA3 and TCA4 for right finger). Each TCA has a length of 100 mm. Considering the actuation force that can be generated by a TCA as well as the required triggering force for AB modules obtained from the characterization, we choose $\theta = 50°$ for each finger. The two fingers are attached to a rigid base to fix their locations. The final gripper except
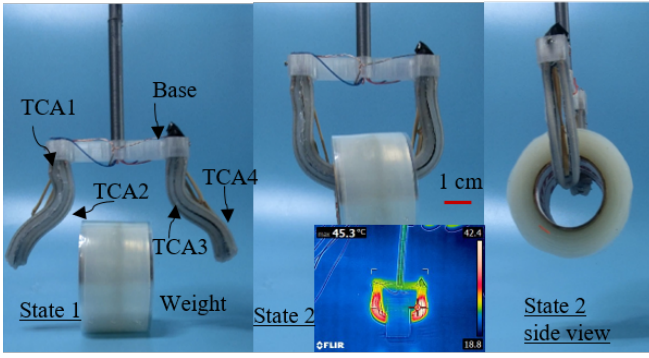
10086

Fig. 7: Gripping 34g with the actuated TCAs.

the base weighs about 4.2 g, but it can hold 34 g, more than eight times its own weight.

Assuming the gripper is initially open, we can close the gripper by applying a 1.5 A current to TCA2 and TCA3 for 0.8 s. To open the gripper, we can apply 1.5 A to TCA1 and TCA4 for 1.5 s. We demonstrate that the gripper can hold a weight of 15 g without energy input and hold 34 g if we apply 0.2 A to TCA2 and TCA3. It can potentially hold more when we applied a larger current. However, a gripper using traditional bending modules as fingers cannot hold the 34 g weight even when a current of 0.5 A is applied to TCA2 and TCA3 (see the supporting video). We record the temperature of the gripper using a thermal camera (E8, FLIR Systems, Inc), and the image with the highest temperature (45.3°C) is shown in the inset of Fig. 7.

B. A Soft Jumping Robot with One Bistable Bending Module

To demonstrate the capability of fast motion, we design a soft jumping robot with one bistable bending module. It's in general more difficult to achieve jumping for a soft robot than a rigid one because a soft robot deforms when contacting the ground, absorbing a certain amount of energy. This difficulty, on the other hand, allows soft robots to withstand impact forces to protect them from damage. Here we demonstrate our soft robot can achieve a dynamic jumping motion relying on a sudden release of the stored energy.

Note that bistable mechanisms have been leveraged for jumping, including mechanisms with multi-link and multi-springs [22]–[24] and closed elastica [25]. Although similar to a closed elastica, our soft robot also has a continuum body, the main difference between our design and the closed elastica is that the closed elastica store all its energy in its flexible body, while our soft robot stores energy both in the spring and its soft body. The reason for such a design is that only the deformation of the body cannot provide enough energy for jumping.

To achieve a larger jumping height, we come up with the following design strategy: (1) decrease energy lost in contact with the ground; (2) store more energy for jumping. To decrease energy lost in collision, one side of the soft body is removed to make the stiffer spine contact with the ground during take-off. Since the stored energy for jumping
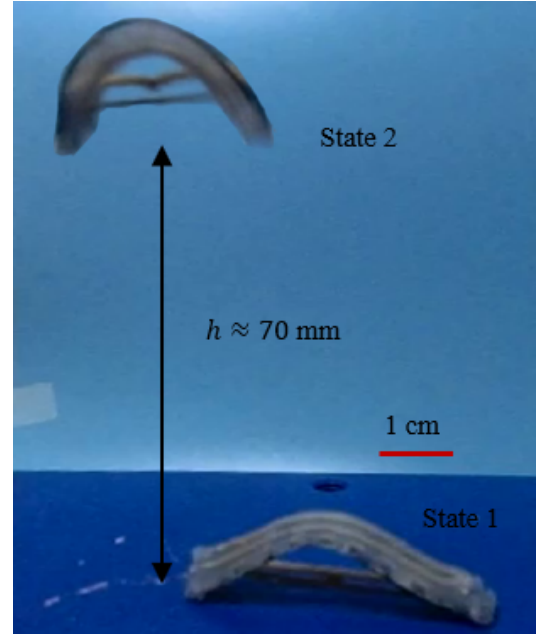

Fig. 8: The jumping experiments.

is positively related to the deformation of the spine and the soft body, the spine with a thickness of 0.5 mm and an initial angle of 75° are used.

For jumping experiments, we manually set the module to state 1 and apply a current of 2.5 A to the TCA for 0.3 s. We use a high-speed camera to record the jumping process and analyze the jumping height from the recorded video. The maximum jumping height for the robot is around 70 mm, which is more than 5 times its body height in state 1. In the experiments, the module needs to be manually set to the state 1, but this can be fixed by keeping the other part of the soft body removed previously. In this case, the robot's jumping height will be reduced as the weight increases, and the soft body will contact the ground during jumping.

VI. CONCLUSIONS

In this work, we propose a design strategy to tune the energy landscape of soft robots for fast and strong motion. We illustrate the design principle with a soft bistable module. Experimental results verified the FEA model and showed the influence of the initial angle on the triggering force. We also demonstrate the usefulness of the proposed strategy by designing a soft gripper and a jumping robot. The gripper can passively hold an object without energy input, and the jumping robot can jump 5 times of its body height.

In the future, we will conduct comprehensive experiments to characterize other parameters that will influence the triggering force (e.g., the thickness of the spine). We will also establish analytical models that include TCA actuations and soft body deformation to predict the performance of the bistable modules driven by TCAs.

REFERENCES

[1] D. Rus and M. T. Tolley, "Design, fabrication and control of soft robots," *Nature*, vol. 521, no. 7553, pp. 467–475, May 2015, insight.

[2] H.-T. Lin, G. G. Leisk, and B. Trimmer, "Goqbot: a caterpillar-inspired soft-bodied rolling robot," *Bioinspiration & biomimetics*, vol. 6, no. 2, p. 026007, 2011.

[3] X. Huang, K. Kumar, M. K. Jawed, A. Mohammadi Nasab, Z. Ye, W. Shan, and C. Majidi, "Highly dynamic shape memory alloy actuator for fast moving soft robots," *Advanced Materials Technologies*, vol. 4, no. 4, p. 1800540, 2019.

[4] F. Ni, D. Rojas, K. Tang, L. Cai, and T. Asfour, "A jumping robot using soft pneumatic actuator," in *2015 IEEE International Conference on Robotics and Automation (ICRA)*. IEEE, 2015, pp. 3154–3159.

[5] M. T. Tolley, R. F. Shepherd, M. Karpelson, N. W. Bartlett, K. C. Galloway, M. Wehner, R. Nunes, G. M. Whitesides, and R. J. Wood, "An untethered jumping soft robot," in *2014 IEEE/RSJ International Conference on Intelligent Robots and Systems*. IEEE, 2014, pp. 561–566.

[6] N. W. Bartlett, M. T. Tolley, J. T. Overvelde, J. C. Weaver, B. Mosadegh, K. Bertoldi, G. M. Whitesides, and R. J. Wood, "A 3d-printed, functionally graded soft robot powered by combustion," *Science*, vol. 349, no. 6244, pp. 161–165, 2015.

[7] J. A. Faber, A. F. Arrieta, and A. R. Studart, "Bioinspired spring origami," *Science*, vol. 359, no. 6382, pp. 1386–1391, 2018.

[8] S. Mintchev, J. Shintake, and D. Floreano, "Bioinspired dual-stiffness origami," *Science Robotics*, vol. 3, no. 20, p. eaau0275, 2018.

[9] Z. Zhai, Y. Wang, and H. Jiang, "Origami-inspired, on-demand deployable and collapsible mechanical metamaterials with tunable stiffness," *Proceedings of the National Academy of Sciences*, vol. 115, no. 9, pp. 2032–2037, 2018.

[10] S. Shan, S. H. Kang, J. R. Raney, P. Wang, L. Fang, F. Candido, J. A. Lewis, and K. Bertoldi, "Multistable architected materials for trapping elastic strain energy," *Advanced Materials*, vol. 27, no. 29, pp. 4296–4301, 2015.

[11] P. Rothemund, A. Ainla, L. Belding, D. J. Preston, S. Kurihara, Z. Suo, and G. M. Whitesides, "A soft, bistable valve for autonomous control of soft actuators," *Science Robotics*, vol. 3, no. 16, p. eaar7986, 2018.

[12] T. Chen, O. R. Bilal, K. Shea, and C. Daraio, "Harnessing bistability for directional propulsion of soft, untethered robots," *Proceedings of the National Academy of Sciences*, vol. 115, no. 22, pp. 5698–5702, 2018.

[13] L. L. Howell, *Compliant mechanisms*. John Wiley & Sons, 2001.

[14] B. Pawlowski, J. Sun, J. Xu, Y. Liu, and J. Zhao, "Modeling of soft robots actuated by twisted-and-coiled actuators," *IEEE/ASME Transactions on Mechatronics*, vol. 24, no. 1, pp. 5–15, 2019.

[15] A. Abbas and J. Zhao, "A physics based model for twisted and coiled actuator," in *Robotics and Automation (ICRA), 2017 IEEE International Conference on*. IEEE, 2017, pp. 6121–6126.

[16] S. I. Rich, R. J. Wood, and C. Majidi, "Untethered soft robotics," *Nature Electronics*, vol. 1, no. 2, p. 102, 2018.

[17] J. Zhao, J. Xu, B. Gao, N. Xi, F. J. Cintron, M. W. Mutka, and L. Xiao, "Msu jumper: A single-motor-actuated miniature steerable jumping robot," *IEEE Transactions on Robotics*, vol. 29, no. 3, pp. 602–614, 2013.

[18] J. Sun, B. Pawlowski, and J. Zhao, "Embedded and controllable shape morphing with twisted-and-coiled actuators*," in *2018 IEEE/RSJ International Conference on Intelligent Robots and Systems (IROS)*, Oct 2018, pp. 5912–5917.

[19] C. S. Haines, M. D. Lima, N. Li, G. M. Spinks, J. Foroughi, J. D. Madden, S. H. Kim, S. Fang, M. J. de Andrade, F. Göktepe, *et al.*, "Artificial muscles from fishing line and sewing thread," *science*, vol. 343, no. 6173, pp. 868–872, 2014.

[20] J. Sun, B. Pawlowski, and J. Zhao, "Soft manipulators with programmable motion using twisted-and-coiled actuators (conference presentation)," in *Electroactive Polymer Actuators and Devices (EAPAD) XXI*, vol. 10966. International Society for Optics and Photonics, 2019, p. 109660Q.

[21] F. Ilievski, A. D. Mazzeo, R. F. Shepherd, X. Chen, and G. M. Whitesides, "Soft robotics for chemists," *Angewandte Chemie International Edition*, vol. 50, no. 8, pp. 1890–1895, 2011.

[22] J.-S. Koh, E. Yang, G.-P. Jung, S.-P. Jung, J. H. Son, S.-I. Lee, P. G. Jablonski, R. J. Wood, H.-Y. Kim, and K.-J. Cho, "Jumping on water: Surface tension–dominated jumping of water striders and robotic insects," *Science*, vol. 349, no. 6247, pp. 517–521, 2015.

[23] S.-P. Jung, G.-P. Jung, J.-S. Koh, D.-Y. Lee, and K.-J. Cho, "Fabrication of composite and sheet metal laminated bistable jumping mechanism," *Journal of Mechanisms and Robotics*, vol. 7, no. 2, p. 021010, 2015.

[24] M. Noh, S.-W. Kim, S. An, J.-S. Koh, and K.-J. Cho, "Flea-inspired catapult mechanism for miniature jumping robots," *IEEE Transactions on Robotics*, vol. 28, no. 5, pp. 1007–1018, 2012.

[25] A. Yamada, M. Watari, H. Mochiyama, and H. Fujimoto, "An asymmetric robotic catapult based on the closed elastica for jumping robot," in *2008 IEEE International Conference on Robotics and Automation*. IEEE, 2008, pp. 232–237.